

# Extended Very-High-Energy Gamma-ray Emission Surrounding PSR J0622 + 3749 Observed by LHAASO-KM2A

F. Aharonian<sup>26,27</sup>, Q. An<sup>4,5</sup>, Axikegu<sup>20</sup>, L.X. Bai<sup>21</sup>, Y.X. Bai<sup>1,3</sup>, Y.W. Bao<sup>15</sup>, D. Bastieri<sup>10</sup>, X.J. Bi<sup>1,2,3</sup>, Y.J. Bi<sup>1,3</sup>, H. Cai<sup>23</sup>, J.T. Cai<sup>10</sup>, Z. Cao<sup>1,2,3</sup>, Z. Cao<sup>4,5</sup>, J. Chang<sup>16</sup>, J.F. Chang<sup>1,3,4</sup>, X.C. Chang<sup>1,3</sup>, B.M. Chen<sup>13</sup>, J. Chen<sup>21</sup>, L. Chen<sup>1,2,3</sup>, L. Chen<sup>18</sup>, L. Chen<sup>20</sup>, M.J. Chen<sup>1,3</sup>, M.L. Chen<sup>1,3,4</sup>, Q.H. Chen<sup>20</sup>, S.H. Chen<sup>1,2,3</sup>, S.Z. Chen<sup>1,3</sup>, T.L. Chen<sup>22</sup>, X.L. Chen<sup>1,2,3</sup>, Y. Chen<sup>15</sup>, N. Cheng<sup>1,3</sup>, Y.D. Cheng<sup>1,3</sup>, S.W. Cui<sup>13</sup>, X.H. Cui<sup>7</sup>, Y.D. Cui<sup>11</sup>, B.Z. Dai<sup>24</sup>, H.L. Dai<sup>1,3,4</sup>, Z.G. Dai<sup>15</sup>, Danzengluobu<sup>22</sup>, D. della Volpe<sup>31</sup>, B. D’Ettorre Piazzoli<sup>28</sup>, X.J. Dong<sup>1,3</sup>, J.H. Fan<sup>10</sup>, Y.Z. Fan<sup>16</sup>, Z.X. Fan<sup>1,3</sup>, J. Fang<sup>24</sup>, K. Fang<sup>1,3</sup>, C.F. Feng<sup>17</sup>, L. Feng<sup>16</sup>, S.H. Feng<sup>1,3</sup>, Y.L. Feng<sup>16</sup>, B. Gao<sup>1,3</sup>, C.D. Gao<sup>17</sup>, Q. Gao<sup>22</sup>, W. Gao<sup>17</sup>, M.M. Ge<sup>24</sup>, L.S. Geng<sup>1,3</sup>, G.H. Gong<sup>6</sup>, Q.B. Gou<sup>1,3</sup>, M.H. Gu<sup>1,3,4</sup>, J.G. Guo<sup>1,2,3</sup>, X.L. Guo<sup>20</sup>, Y.Q. Guo<sup>1,3</sup>, Y.Y. Guo<sup>1,2,3,16</sup>, Y.A. Han<sup>14</sup>, H.H. He<sup>1,2,3</sup>, H.N. He<sup>16</sup>, J.C. He<sup>1,2,3</sup>, S.L. He<sup>10</sup>, X.B. He<sup>11</sup>, Y. He<sup>20</sup>, M. Heller<sup>31</sup>, Y.K. Hor<sup>11</sup>, C. Hou<sup>1,3</sup>, X. Hou<sup>25</sup>, H.B. Hu<sup>1,2,3</sup>, S. Hu<sup>21</sup>, S.C. Hu<sup>1,2,3</sup>, X.J. Hu<sup>6</sup>, D.H. Huang<sup>20</sup>, Q.L. Huang<sup>1,3</sup>, W.H. Huang<sup>17</sup>, X.T. Huang<sup>17</sup>, Z.C. Huang<sup>20</sup>, F. Ji<sup>1,3</sup>, X.L. Ji<sup>1,3,4</sup>, H.Y. Jia<sup>20</sup>, K. Jiang<sup>4,5</sup>, Z.J. Jiang<sup>24</sup>, C. Jin<sup>1,2,3</sup>, D. Kuleshov<sup>29</sup>, K. Levochkin<sup>29</sup>, B.B. Li<sup>13</sup>, C. Li<sup>1,3</sup>, C. Li<sup>4,5</sup>, F. Li<sup>1,3,4</sup>, H.B. Li<sup>1,3</sup>, H.C. Li<sup>1,3</sup>, H.Y. Li<sup>5,16</sup>, J. Li<sup>1,3,4</sup>, K. Li<sup>1,3</sup>, W.L. Li<sup>17</sup>, X. Li<sup>4,5</sup>, X. Li<sup>20</sup>, X.R. Li<sup>1,3</sup>, Y. Li<sup>21</sup>, Y.Z. Li<sup>1,2,3</sup>, Z. Li<sup>1,3</sup>, Z. Li<sup>9</sup>, E.W. Liang<sup>12</sup>, Y.F. Liang<sup>12</sup>, S.J. Lin<sup>11</sup>, B. Liu<sup>5</sup>, C. Liu<sup>1,3</sup>, D. Liu<sup>17</sup>, H. Liu<sup>20</sup>, H.D. Liu<sup>14</sup>, J. Liu<sup>1,3</sup>, J.L. Liu<sup>19</sup>, J.S. Liu<sup>11</sup>, J.Y. Liu<sup>1,3</sup>, M.Y. Liu<sup>22</sup>, R.Y. Liu<sup>15</sup>, S.M. Liu<sup>16</sup>, W. Liu<sup>1,3</sup>, Y.N. Liu<sup>6</sup>, Z.X. Liu<sup>21</sup>, W.J. Long<sup>20</sup>, R. Lu<sup>24</sup>, H.K. Lv<sup>1,3</sup>, B.Q. Ma<sup>9</sup>, L.L. Ma<sup>1,3</sup>, X.H. Ma<sup>1,3</sup>, J.R. Mao<sup>25</sup>, A. Masood<sup>20</sup>, W. Mitthumsiri<sup>32</sup>, T. Montaruli<sup>31</sup>, Y.C. Nan<sup>17</sup>, B.Y. Pang<sup>20</sup>, P. Pattarakijwanich<sup>32</sup>, Z.Y. Pei<sup>10</sup>, M.Y. Qi<sup>1,3</sup>, D. Ruffolo<sup>32</sup>, V. Rudev<sup>29</sup>, A. Sáiz<sup>32</sup>, L. Shao<sup>13</sup>, O. Shchegolev<sup>29,30</sup>, X.D. Sheng<sup>1,3</sup>, J.R. Shi<sup>1,3</sup>, H.C. Song<sup>9</sup>, Yu.V. Stenkin<sup>29,30</sup>, V. Stepanov<sup>29</sup>, Q.N. Sun<sup>20</sup>, X.N. Sun<sup>12</sup>, Z.B. Sun<sup>8</sup>, P.H.T. Tam<sup>11</sup>, Z.B. Tang<sup>4,5</sup>, W.W. Tian<sup>2,7</sup>, B.D. Wang<sup>1,3</sup>, C. Wang<sup>8</sup>, H. Wang<sup>20</sup>, H.G. Wang<sup>10</sup>, J.C. Wang<sup>25</sup>, J.S. Wang<sup>19</sup>, L.P. Wang<sup>17</sup>, L.Y. Wang<sup>1,3</sup>, R.N. Wang<sup>20</sup>, W. Wang<sup>11</sup>, W. Wang<sup>23</sup>, X.G. Wang<sup>12</sup>, X.J. Wang<sup>1,3</sup>, X.Y. Wang<sup>15</sup>, Y.D. Wang<sup>1,3</sup>, Y.J. Wang<sup>1,3</sup>, Y.P. Wang<sup>1,2,3</sup>, Z. Wang<sup>1,3,4</sup>, Z. Wang<sup>19</sup>, Z.H. Wang<sup>21</sup>, Z.X. Wang<sup>24</sup>, D.M. Wei<sup>16</sup>, J.J. Wei<sup>16</sup>, Y.J. Wei<sup>1,2,3</sup>, T. Wen<sup>24</sup>, C.Y. Wu<sup>1,3</sup>, H.R. Wu<sup>1,3</sup>, S. Wu<sup>1,3</sup>, W.X. Wu<sup>20</sup>, X.F. Wu<sup>16</sup>, S.Q. Xi<sup>20</sup>, J. Xia<sup>5,16</sup>, J.J. Xia<sup>20</sup>, G.M. Xiang<sup>2,18</sup>, G. Xiao<sup>1,3</sup>, H.B. Xiao<sup>10</sup>, G.G. Xin<sup>23</sup>, Y.L. Xin<sup>20</sup>, Y. Xing<sup>18</sup>, D.L. Xu<sup>19</sup>, R.X. Xu<sup>9</sup>, L. Xue<sup>17</sup>, D.H. Yan<sup>25</sup>, C.W. Yang<sup>21</sup>, F.F. Yang<sup>1,3,4</sup>, J.Y. Yang<sup>11</sup>, L.L. Yang<sup>11</sup>, M.J. Yang<sup>1,3</sup>, R.Z. Yang<sup>5</sup>, S.B. Yang<sup>24</sup>, Y.H. Yao<sup>21</sup>, Z.G. Yao<sup>1,3</sup>, Y.M. Ye<sup>6</sup>, L.Q. Yin<sup>1,3</sup>, N. Yin<sup>17</sup>, X.H. You<sup>1,3</sup>, Z.Y. You<sup>1,2,3</sup>, Y.H. Yu<sup>17</sup>, Q. Yuan<sup>16</sup>, H.D. Zeng<sup>16</sup>, T.X. Zeng<sup>1,3,4</sup>, W. Zeng<sup>24</sup>, Z.K. Zeng<sup>1,2,3</sup>, M. Zha<sup>1,3</sup>, X.X. Zhai<sup>1,3</sup>, B.B. Zhang<sup>15</sup>, H.M. Zhang<sup>15</sup>, H.Y. Zhang<sup>17</sup>, J.L. Zhang<sup>7</sup>, J.W. Zhang<sup>21</sup>, L. Zhang<sup>13</sup>, L. Zhang<sup>24</sup>, L.X. Zhang<sup>10</sup>, P.F. Zhang<sup>24</sup>, P.P. Zhang<sup>13</sup>, R. Zhang<sup>5,16</sup>, S.R. Zhang<sup>13</sup>, S.S. Zhang<sup>1,3</sup>, X. Zhang<sup>15</sup>, X.P. Zhang<sup>1,3</sup>, Y. Zhang<sup>1,3</sup>, Y. Zhang<sup>1,16</sup>, Y.F. Zhang<sup>20</sup>, Y.L. Zhang<sup>1,3</sup>, B. Zhao<sup>20</sup>, J. Zhao<sup>1,3</sup>, L. Zhao<sup>4,5</sup>, L.Z. Zhao<sup>13</sup>, S.P. Zhao<sup>16,17</sup>, F. Zheng<sup>8</sup>, Y. Zheng<sup>20</sup>, B. Zhou<sup>1,3</sup>, H. Zhou<sup>19</sup>, J.N. Zhou<sup>18</sup>, P. Zhou<sup>15</sup>, R. Zhou<sup>21</sup>, X.X. Zhou<sup>20</sup>, C.G. Zhu<sup>17</sup>, F.R. Zhu<sup>20</sup>, H. Zhu<sup>7</sup>, K.J. Zhu<sup>1,2,3,4</sup>, X. Zuo<sup>1,3</sup> (LHAASO Collaboration)\* and X.Y. Huang<sup>16</sup>

<sup>1</sup>Key Laboratory of Particle Astrophysics & Experimental Physics Division & Computing Center, Institute of High Energy Physics, Chinese Academy of Sciences, 100049 Beijing, China

<sup>2</sup>University of Chinese Academy of Sciences, 100049 Beijing, China

<sup>3</sup>TIANFU Cosmic Ray Research Center, Chengdu, Sichuan, China

<sup>4</sup>State Key Laboratory of Particle Detection and Electronics, China

<sup>5</sup>University of Science and Technology of China, 230026 Hefei, Anhui, China

<sup>6</sup>Department of Engineering Physics, Tsinghua University, 100084 Beijing, China

<sup>7</sup>National Astronomical Observatories, Chinese Academy of Sciences, 100101 Beijing, China

<sup>8</sup>National Space Science Center, Chinese Academy of Sciences, 100190 Beijing, China

<sup>9</sup>School of Physics, Peking University, 100871 Beijing, China

<sup>10</sup>Center for Astrophysics, Guangzhou University, 510006 Guangzhou, Guangdong, China

<sup>11</sup>School of Physics and Astronomy & School of Physics (Guangzhou), Sun Yat-sen University, 519082 Zhuhai, Guangdong, China

<sup>12</sup>School of Physical Science and Technology, Guangxi University, 530004 Nanning, Guangxi, China

<sup>13</sup>Hebei Normal University, 050024 Shijiazhuang, Hebei, China

<sup>14</sup>School of Physics and Microelectronics, Zhengzhou University, 450001 Zhengzhou, Henan, China

<sup>15</sup>School of Astronomy and Space Science, Nanjing University, 210023 Nanjing, Jiangsu, China

<sup>16</sup>Key Laboratory of Dark Matter and Space Astronomy, Purple Mountain Observatory, Chinese Academy of Sciences, 210023 Nanjing, Jiangsu, China

<sup>17</sup>Institute of Frontier and Interdisciplinary Science, Shandong University, 266237 Qingdao, Shandong, China

<sup>18</sup>Key Laboratory for Research in Galaxies and Cosmology, Shanghai Astronomical Observatory, Chinese Academy of Sciences, 200030 Shanghai, China

<sup>19</sup>Key Laboratory of Particle Astrophysics & Experimental Physics Division & Computing Center, Institute of High Energy Physics, Chinese Academy of Sciences, 100049 Beijing, China

<sup>19</sup>*Tsung-Dao Lee Institute & School of Physics and Astronomy,  
Shanghai Jiao Tong University, 200240 Shanghai, China*

<sup>20</sup>*School of Physical Science and Technology & School of Information Science and Technology,  
Southwest Jiaotong University, 610031 Chengdu, Sichuan, China*

<sup>21</sup>*College of Physics, Sichuan University, 610065 Chengdu, Sichuan, China*

<sup>22</sup>*Key Laboratory of Cosmic Rays (Tibet University), Ministry of Education, 850000 Lhasa, Tibet, China*

<sup>23</sup>*School of Physics and Technology, Wuhan University, 430072 Wuhan, Hubei, China*

<sup>24</sup>*School of Physics and Astronomy, Yunnan University, 650091 Kunming, Yunnan, China*

<sup>25</sup>*Yunnan Observatories, Chinese Academy of Sciences, 650216 Kunming, Yunnan, China*

<sup>26</sup>*Dublin Institute for Advanced Studies, 31 Fitzwilliam Place, 2 Dublin, Ireland*

<sup>27</sup>*Max-Planck-Institut für Nuclear Physics, P.O. Box 103980, 69029 Heidelberg, Germany*

<sup>28</sup>*Dipartimento di Fisica dell'Università di Napoli "Federico II",*

*Complesso Universitario di Monte Sant'Angelo, via Cinthia, 80126 Napoli, Italy.*

<sup>29</sup>*Institute for Nuclear Research of Russian Academy of Sciences, 117312 Moscow, Russia*

<sup>30</sup>*Moscow Institute of Physics and Technology, 141700 Moscow, Russia*

<sup>31</sup>*Département de Physique Nucléaire et Corpusculaire, Faculté de Sciences,  
Université de Genève, 24 Quai Ernest Ansermet, 1211 Geneva, Switzerland*

<sup>32</sup>*Department of Physics, Faculty of Science, Mahidol University, 10400 Bangkok, Thailand and*

(Dated: June 18, 2021)

We report the discovery of an extended very-high-energy (VHE) gamma-ray source around the location of the middle-aged (207.8 kyr) pulsar PSR J0622+3749 with the Large High Altitude Air Shower Observatory (LHAASO). The source is detected with a significance of  $8.2\sigma$  for  $E > 25$  TeV assuming a Gaussian template. The best-fit location is (R.A., Dec.) =  $(95^\circ.47 \pm 0^\circ.11, 37^\circ.92 \pm 0^\circ.09)$ , and the extension is  $0^\circ.40 \pm 0^\circ.07$ . The energy spectrum can be described by a power-law spectrum with an index of  $-2.92 \pm 0.17_{\text{stat}} \pm 0.02_{\text{sys}}$ . No clear extended multi-wavelength counterpart of the LHAASO source has been found from the radio to sub-TeV bands. The LHAASO observations are consistent with the scenario that VHE electrons escaped from the pulsar, diffused in the interstellar medium, and scattered the interstellar radiation field. If interpreted as the pulsar halo scenario, the diffusion coefficient, inferred for electrons with median energies of  $\sim 160$  TeV, is consistent with those obtained from the extended halos around Geminga and Monogem and much smaller than that derived from cosmic ray secondaries. The LHAASO discovery of this source thus likely enriches the class of so-called pulsar halos and confirms that high-energy particles generally diffuse very slowly in the disturbed medium around pulsars.

PACS numbers: 96.50.S-, 96.50.sb, 98.70.Sa

## I. INTRODUCTION

Charged cosmic rays (CRs) are known to propagate diffusively in the random magnetic field of the Milky Way. The diffusion coefficient, which relies on the properties of the turbulent interstellar medium (ISM), is a key parameter governing the propagation of CRs. Through measuring the secondary-to-primary ratios of CR nuclei, the average diffusion coefficient of the Milky Way can be inferred [1, 2]. While the propagation of CRs is naturally expected to be inhomogeneous, the simple uniform and isotropic diffusion model can account for most of the measurements of CRs and diffuse  $\gamma$  rays [3].

Recently, the HAWC collaboration reported the observations of extended very-high-energy (VHE)  $\gamma$ -ray emission from two middle-aged, isolated pulsars, Geminga and Monogem [4]. The spatial morphologies of the  $\gamma$ -ray emission indicate that the diffusion of particles in the regions around those pulsars are much slower than the average value to give enough secondary particle yields [2, 5]. These results suggest that the diffusion of particles in the Milky Way is very likely inhomogeneous [6–9].

Such extended halos around middle-aged pulsars<sup>1</sup> may be common at VHE energies [14–16], which was actually predicted a long time ago [17]. Pulsar halos may even contribute to the diffuse emission at TeV energies [17–19]. The cause of the slow diffusion is yet to be elucidated but might be due to specific properties of the magnetic turbulence around the pulsar [20–22].

Here we report the detection of LHAASO J0621+3755, an extended  $\gamma$ -ray source with energies above 10 TeV, with half array of the LHAASO experiment. In the third HAWC source catalog, a source with similar coordinates, 3HWC J0621+382, was reported recently [23]. No source with similar coordinate was shown in the second HAWC source catalog [24]. However, the nearest Fermi source of 3HWC J0621+382 was found to be the blazar 4FGL J0620.3+3804. LHAASO J0621+3755 is positionally coincident with the  $\gamma$ -ray pulsar J0622+3749 discovered by Fermi-LAT [25]. The period of PSR J0622+3749 is about 0.333 s, the spin-down luminosity is  $2.7 \times 10^{34}$  erg s<sup>-1</sup>, and the characteristic age is about 207.8 kyr. No precise distance measurement of the pulsar

\* E-mail: fengyl@pmo.ac.cn, yuanq@pmo.ac.cn, zhangyi@pmo.ac.cn, zhuhui@bao.ac.cn

<sup>1</sup> Note that different definitions of pulsar halos exist in the literature [10, 11]. For example, some young pulsars that exhibit particle escape are also called pulsar halos [12, 13].

is available now. A “pseudo distance” of 1.6 kpc was given via the correlation between the  $\gamma$ -ray luminosity and the spin-down power for  $\gamma$ -ray pulsars [26]. The VHE  $\gamma$ -ray and multi-wavelength properties of LHAASO J0621+3755 have been studied, which suggest that this source is very likely a pulsar halo similar to Geminga and Monogem observed by HAWC [4].

## II. LHAASO-KM2A OBSERVATIONS

### A. The LHAASO experiment

LHAASO is a hybrid, large area, wide field-of-view observatory for CRs and  $\gamma$  rays in a wide energy range. LHAASO serves as the most sensitive  $\gamma$ -ray detector for energies above a few tens of TeV, and is expected to give revolutionary insights in the VHE domain of astroparticle physics, such as the origin and propagation of CRs, as well as the nature of VHE  $\gamma$ -ray sources. KM2A is the main array of LHAASO, with an area of  $\sim 1.3$  km<sup>2</sup>, consisting of 5195 electromagnetic detectors (EDs) and 1188 muon detectors (MDs). See the Supplemental Material [27] for the detector configuration.

LHAASO’s first observation on the Crab Nebula is presented in [39]. By the measurements of this standard candle, detailed studies of the detector performance have been carried out, including angular resolution, pointing accuracy and cosmic-ray background rejection power. The pipeline of data analysis and Monte-Carlo (MC) simulations was then constructed. In this paper, we adopt the same simulation procedure and get the MC data sample of  $2.2 \times 10^8$   $\gamma$ -ray events as described in Ref. [39].

### B. Analysis method

Data used in this analysis were collected by the half array of KM2A, from December 27, 2019 to November 9, 2020, with a live time of 281.9 days. The directions of  $\gamma$  rays are reconstructed using the arrival time and deposited energy recorded by each ED. The angular resolution (68% containment) is  $0^\circ.5 - 0^\circ.8$  at 20 TeV and  $0^\circ.24 - 0^\circ.30$  at 100 TeV, depending on the declination of incident photons. The maximum zenith angle of events was chosen as  $50^\circ$ . Event selection conditions are consistent with those in the Crab Nebula analysis [39], and more details can be found in the Supplemental Material [27].

KM2A uses  $\rho_{50}$ , defined as the particle density in the best-fit Nishimura-Kamata-Greisen (NKG; [40]) function at a perpendicular distance of 50 m from the shower axis, to estimate the primary energy of a  $\gamma$ -ray event. This parameter is a robust energy estimator, because it utilizes the whole knowledge of the lateral distribution function of a shower [39, 41, 42]. For showers with zenith angles less than  $20^\circ$ , the energy resolution is about 24% at 20 TeV and 13% at 100 TeV [39].

Because a high-energy  $\gamma$ -ray-induced shower has fewer muons than a CR-induced shower, we use the ratio  $N_\mu/N_e$  to

discriminate  $\gamma$  rays from the CR background, where  $N_\mu$  is the total number of muons collected by MDs and  $N_e$  is the total number of particles counted by EDs. The criteria of this ratio were optimized using the MC events of  $\gamma$ -ray photons and the real CR data. KM2A is capable of rejecting the CR background by 99% at 20 TeV and 99.99% above 100 TeV, while maintaining a 90% efficiency for  $\gamma$  rays [39].

The sky around the target source is binned into cells with a size of  $0^\circ.1$  in both the right ascension (R.A.) and declination (Dec.) directions. The background map is estimated by the equi-zenith angle method [43, 44]. In brief, for a candidate source, the background is estimated by collecting events in the same zenith angle belt, after excluding events from the source region. The radius of the source region is defined as three times the width of a Gaussian function, which is the convolution of the point-spread function (PSF) and the source extension. This method can eliminate various detection effects caused by the instrumental and environmental variations. Another widely used method is the so-called direct integration method [39], which estimates the background using the events in the same directions in horizontal coordinate but different arrival times. A cross check of the two methods showed no noticeable difference.

The significance of the source was estimated using a test statistic variable as two times of the logarithmic likelihood ratio, i.e.,  $TS = 2 \ln(\mathcal{L}_{s+b}/\mathcal{L}_b)$ , where  $\mathcal{L}_{s+b}$  is the maximum likelihood for the signal plus background hypothesis and  $\mathcal{L}_b$  is the likelihood for the background only hypothesis. According to the Wilks’ theorem [45], in the background only case, the TS value follows a  $\chi^2$  distribution with  $n$  degrees of freedom, where  $n$  is the number of free parameters in the signal model. In the case of a point source with fixed position, which has only one free parameter (the normalization when ignoring the spectral distribution), the pre-trial significance is  $\sqrt{TS}$ .

We use a binned-likelihood, forward-folding procedure to measure the spectral energy distribution (SED) of this source. The number of  $\gamma$ -ray events is counted in three bins with a width of  $\Delta \log_{10} E = 0.4$  (instead of 0.2 as in Ref. [39]) to give a higher significance in each bin ranging from 10 TeV to 160 TeV. The SED of the source is assumed to follow a power-law spectrum  $dN/dE = \phi_0 \times (E/E_0)^{-\gamma}$ , where  $E_0 = 40$  TeV is a reference energy. The best-fit values of  $\phi_0$  and  $\gamma$  are obtained via the maximum likelihood algorithm.

### C. Results

Fig. 1 shows the  $3^\circ \times 3^\circ$  significance map around PSR J0622 + 3749 with energies above 25 TeV in the equatorial coordinates. This map is smoothed with the PSF, the 68% containment radius of which is  $0^\circ.45$  in this energy range, as indicated by the white circle in Fig.1.

We use four spatial templates, convolved with the PSF, to study the morphology of the source: point source, two-dimensional Gaussian model, uniform disk, and the diffusion model from a point source with constant injection rate [4]. Table I lists the best-fit source positions, extensions, and the TS values for these templates. For the point source assumption,

the fit to the  $> 25$  TeV skymap gives a  $TS$  value of 63.0.

In the case of the two-dimensional Gaussian model, the fit yields R.A. =  $95^{\circ}.47 \pm 0^{\circ}.11$ , Dec. =  $37^{\circ}.92 \pm 0^{\circ}.09$ , and extension  $\sigma = 0^{\circ}.40 \pm 0^{\circ}.07$ . The centroid of LHAASO J0621+3755 is consistent with the location of Fermi-LAT pulsar J0622+3749, with in an angular distance of  $0^{\circ}.11 \pm 0^{\circ}.12$ . It is also consistent with the expectation of the pulsar halo model that the  $\gamma$ -ray emission above 10 TeV is close to the pulsar due to the fast cooling of such VHE  $e^{\pm}$ , even if there is a moderate proper motion of the pulsar [46]. The  $TS$  value of the source is 79.5, corresponding to a significance of  $8.2\sigma$  for four free parameters. Assuming a uniform disk model, we obtain a similar significance with a disk radius of  $0^{\circ}.70 \pm 0^{\circ}.10$ .

To study the significance of the extension of the source, we define  $TS_{\text{ext}} = 2 \ln(\mathcal{L}_{\text{ext}}/\mathcal{L}_{\text{ps}})$ , i.e., twice the logarithm of the likelihood ratio of an extended source assumption to a point source assumption [47]. The  $TS_{\text{ext}}$  for the Gaussian template is about 16.5, which corresponds to a significance of  $\sim 4.1\sigma$  for an additional free parameter.

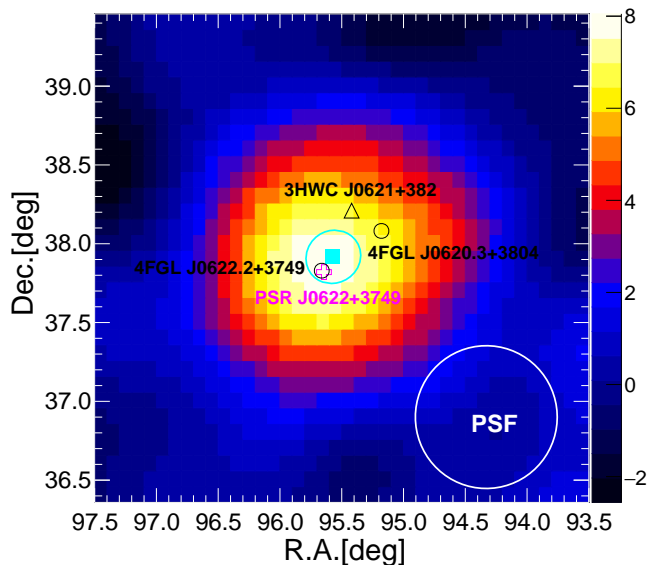


FIG. 1. Significance map of the  $3^{\circ} \times 3^{\circ}$  region around LHAASO J0621+3755 with energy above 25 TeV. The cyan square and circle denote the best-fit and  $1\sigma$  range of the location of the LHAASO source. The triangle marks the location of 3HWC J0621+382, the black circles show the locations of the two 4FGL sources, and the pink cross marks the location of PSR J0622+3749. The angular distance between the centroid of LHAASO J0621+3755 and PSR J0622+3749 is  $0^{\circ}.11 \pm 0^{\circ}.12$ . The white circle at the bottom-right corner shows the size of the LHAASO PSF (68% containment).

To further study the spatial distribution of the source, we use a fitting form of the morphological distribution from a diffusion model under the approximation of continuous injection

from a point source<sup>2</sup>

$$f(\theta) \propto \frac{1}{\theta_d(\theta + 0.085\theta_d)} \exp[-1.54(\theta/\theta_d)^{1.52}], \quad (1)$$

to fit the KM2A observed morphology. In the above equation,  $\theta$  is the angular distance from the source position, and  $\theta_d = \frac{180^{\circ}}{\pi} \cdot \frac{2\sqrt{D(E_e)t_E}}{d}$  is the typical diffusion extension with  $D(E_e)$  as the diffusion coefficient and  $t_E \sim 5.5$  kyr as the cooling time of electrons and positrons with  $\sim 160$  TeV energies (see Sec. F of Supplemental Material [27] for the magnetic field and photon fields used in this work). This formula is a slightly improved version of that introduced in Ref. [4], and can match the numerical calculation, which includes the diffusion of  $e^{\pm}$ , the inverse Compton scattering (ICS) off the background radiation field, and the line-of-sight integral of the  $\gamma$ -ray emission, within a few percent up to a distance as far as  $3\theta_d$  from the central source (see Sec. G of Supplemental Material [27]). We get the fitted  $\theta_d = 0^{\circ}.91 \pm 0^{\circ}.20$  for  $E > 25$  TeV, and the  $TS$  value of 78.1 for the diffusion model, as given in Table I. We have tested via MC simulations that the differences among the three extended templates are not significant (with a largest difference of  $\sim 1.8\sigma$ ). The one-dimensional distribution of the number of events after subtracting the estimated background, together with the fitting  $1\sigma$  band of the diffusion model, are shown in Fig. 2.

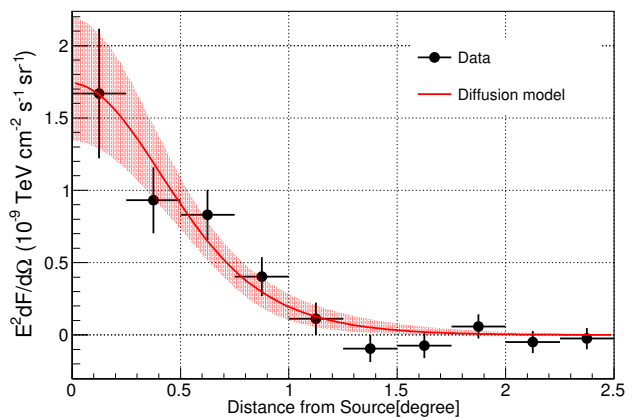


FIG. 2. One-dimensional distribution of the  $> 25$  TeV  $\gamma$ -ray emission of LHAASO J0621+3755. The solid line and shaded band show the best fit and  $\Delta\chi^2 = 2.3$  range of the diffusion model fit, which is the convolution of Eq. (1) with the PSF.

Using the Gaussian extension of  $0^{\circ}.40$ , the resulting differential flux ( $\text{TeV}^{-1} \text{cm}^{-2} \text{s}^{-1}$ ), assuming a single power-law

<sup>2</sup> A more detailed modeling of the emission considering e.g., the injection history and potential pulsar proper motion [9, 48] might lead to small differences of the spatial distribution, and hence the estimate of the extension parameter.

TABLE I. Results of the morphological analyses of LHAASO J0621+3755.

Template	Extension <sup>a</sup> (°)	RA (°)	Dec (°)	$TS$	$N_p^b$
Point source	-	$95.56 \pm 0.10$	$37.85 \pm 0.07$	63.0	3
2D Gaussian	$0.40 \pm 0.07$	$95.47 \pm 0.11$	$37.92 \pm 0.09$	79.5	4
Uniform disk	$0.70 \pm 0.10$	$95.44 \pm 0.11$	$37.94 \pm 0.09$	80.2	4
Diffusion	$0.91 \pm 0.20$	$95.48 \pm 0.10$	$37.90 \pm 0.09$	78.1	4

<sup>a</sup>Radius for the uniform disk;  $\sigma$  for the Gaussian model;  $\theta_d$  for the diffusion model. <sup>b</sup> $N_p$  is the number of parameters in the model.

form, is

$$\frac{dN}{dE} = (3.11 \pm 0.38_{\text{stat}} \pm 0.22_{\text{sys}}) \times 10^{-16} (E/40 \text{ TeV})^{-2.92 \pm 0.17_{\text{stat}} \pm 0.02_{\text{sys}}} \quad (2)$$

We derive the fluxes of LHAASO J0621+3755 in four energy bins, [10, 25], [25 – 63], [63 – 158], and [158 – 398] TeV, respectively. Above 100 TeV, we observed four photon-like events against 0.5 background events, which corresponds to a  $3.1\sigma$  statistical significance. Because the significance in the last energy bin is smaller than  $2\sigma$ , a 95% upper limit is derived. The SED is given in Fig. 3, where the geometric mean energy is used to represent the energy of corresponding bin. Assuming a power-law with an exponential cut-off improves the fitting quality very little, which gives a  $TS$  value higher by 1.6 but with one more free parameter.

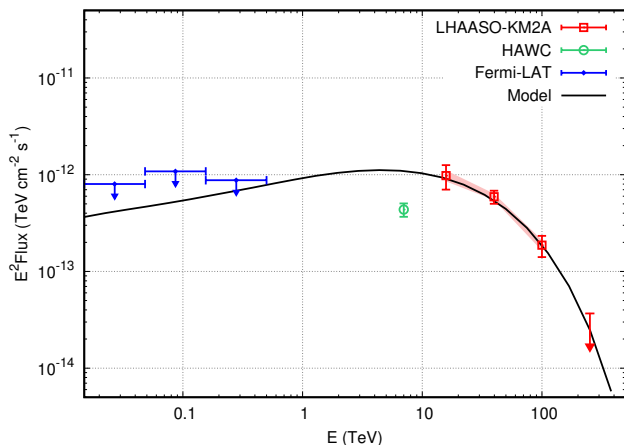


FIG. 3. The spectrum of LHAASO J0621+3755. The error bars represent statistical uncertainties, and the shaded band shows the systematic uncertainties. The HAWC measurement of 3HWC J0621+382 [23] and the Fermi-LAT 95% upper limits are also shown. The line shows the prediction based on the pulsar halo model (see Sec. IV).

### III. MULTI-WAVELENGTH STUDIES

LHAASO J0621+3755 is a new source in the VHE domain, without a counterpart in the TeVCat<sup>3</sup> [49]. It is potentially associated with 3HWC J0621+382 in the third HAWC catalog [23], since the angular distance between two sources is  $0.31^\circ \pm 0.32^\circ$ . In the GeV energy band, we find two 4FGL sources [50], 4FGL J0622.2+3749 and 4FGL J0620.3+3804, in the vicinity of LHAASO J0621+3755 (see Fig. 1). 4FGL J0620.3+3804 is associated with the radio source GB6 J0620+3806 [51], and is classified as a “bcu” (blazar candidate of uncertain type) in the 4FGL catalog [50]. Since LHAASO J0621+3755 shows emission up to 100 TeV energies, we expect that it should not be associated with 4FGL J0620.3+3804. The other source, 4FGL J0622.2+3749, is a  $\gamma$ -ray pulsar discovered using the Fermi-LAT data [25]. Multi-wavelength counterparts of the pulsar have been searched for in Ref. [25]. No X-ray or pulsed radio emission has been found. Faint sources and extended diffuse emission might exist in the MPIfR surveys of radio continuum emission at 408 MHz and 1420 MHz [52, 53]. However, after checking the 820 MHz and 4850 MHz images [54, 55], we find no clear diffuse emission around the pulsar (see Fig.S1 in the Supplemental Material [27]). The search in the infrared and optical bands does not reveal counterparts of the pulsar or the extended halo.

The potential extended GeV  $\gamma$ -ray emission can give very useful constraints on the properties of CR injection from the pulsar and diffusion in the ISM [48, 56, 57]. For Geminga, a possible large extended counterpart of the TeV halo was reported in [48]. We therefore analyzed 11.5 years of the Fermi-LAT data to search for extended emission associated with LHAASO J0621+3755. Events of P8R3 version and SOURCE class in a square region of  $25^\circ \times 25^\circ$  with energies between 15 and 500 GeV were used. The diffuse models used are `gll_iem_v07.fits` and `iso_P8R3_SOURCE_V2_v1.txt`<sup>4</sup>. A binned likelihood method is adopted, with background source model XML file generated using `make4FGLxml.py`<sup>5</sup> based on the 4FGL source catalog [50]. No clear extended emission has been found. The 95% flux upper limits have been derived, assuming the predicted spatial template from the diffusion model in the relevant energy band. The results are also shown in Fig. 3. For more details of the Fermi-LAT data analysis, please refer to the Supplemental Material [27].

<sup>3</sup> <http://tevcat.uchicago.edu>

<sup>4</sup> <http://fermi.gsfc.nasa.gov/ssc/data/access/lat/BackgroundModels.html>

<sup>5</sup> <http://fermi.gsfc.nasa.gov/ssc/data/analysis/user/>

#### IV. INTERPRETATION AS A PULSAR HALO

TABLE II. Comparison of the properties of pulsars J0622+3749, Geminga, and Monogem.

Name	$P$ (s)	$\dot{P}$ ( $10^{-14} \text{ s s}^{-1}$ )	$L_{\text{sd}}$ ( $10^{34} \text{ erg s}^{-1}$ )	$\tau$ (kyr)	$d$ (kpc)	Ref.
J0622+3749	0.333	2.542	2.7	207.8	1.60	[25]
Geminga	0.237	1.098	3.3	342.0	0.25	[58]
Monogem	0.385	5.499	3.8	110.0	0.29	[58]

The multi-wavelength search indicates that LHAASO J0621+3755 is a VHE  $\gamma$ -ray-only source possibly associated with PSR J0622+3749. The pulsar is a middle-aged pulsar, similar to those of Geminga and Monogem. In Table II we compare the main properties of PSR J0622+3749 with those of Geminga and Monogem. Note that these three pulsars share similar properties. No clear pulsar wind nebula (PWN) emission is visible in the radio, infrared, optical, and X-ray bands. For Geminga and Monogem, weak PWNe have been shown in the X-ray images [59, 60]. The lack of PWN emission associated with PSR J0622+3749 can be understood in terms of its larger distance. Taking the Monogem PWN as an example, the total unabsorbed 0.5 – 8 keV flux of the extended emission (in a small region with radii from  $3''.5$  to  $15''$ ) is  $8.3^{+5.7}_{-4.4} \times 10^{-15} \text{ erg s}^{-1} \text{ cm}^{-2}$  [60]. Assuming the same level of PWN emission, the potential X-ray PWN associated with PSR J0622+3749 would be too faint given a distance of 1.60/0.29 times larger. The multi-wavelength observational results are thus consistent with the scenario that the VHE  $\gamma$ -ray emission comes from the electrons and positrons diffusing out from the pulsar which then scatter the interstellar radiation field.

With the  $\theta_d$  values inferred from the morphological fitting, we obtain a diffusion coefficient  $D \approx (8.9^{+4.5}_{-3.9}) \times 10^{27} (d/1.6 \text{ kpc})^2 \text{ cm}^2 \text{ s}^{-1}$  for  $E_e \sim 160 \text{ TeV}$ . Here we adopt the approximate scaling relation between electrons and ICS photons  $\bar{E}_e \approx 17 \bar{E}_\gamma^{0.54+0.046 \log(\bar{E}_\gamma/\text{TeV})}$  [4], where  $\bar{E}_\gamma \approx 40 \text{ TeV}$  is the median energy of photons. The diffusion coefficient is comparable to the results derived from observations of Geminga and Monogem [4], which is about  $4.5 \times 10^{27} \text{ cm}^2 \text{ s}^{-1}$  for  $E_e \sim 100 \text{ TeV}$ , and is significantly smaller than that inferred from the CR secondary-to-primary ratios ( $\sim 10^{30} - 10^{31} \text{ cm}^2 \text{ s}^{-1}$ ; [1, 2]). Given the current data statistics, the energy dependence of the diffusion coefficient cannot be robustly determined yet.

We model the wide-band  $\gamma$ -ray SED of LHAASO J0621+3755 with an ICS model of  $e^\pm$  diffusing out from the pulsar or PWN. A two-zone diffusion model [6] is assumed, with a slow-diffusion-coefficient the same as that inferred from the LHAASO observation, a slow-diffusion region size of 50 pc, and a diffusion coefficient 300 times larger outside. The energy-dependence of the diffusion coefficient is assumed to be proportional to  $E^{1/3}$ . A super-exponentially cutoff power-law spectrum,  $q(E) \propto E^{-\alpha} \exp[-(E/E_c)^\beta]$ , is adopted to describe the injection spectrum of  $e^\pm$ . For more details of the model setting one can refer to the Supplemental

Material [27]. The calculated result is shown by the solid line in Fig. 3, with  $\alpha = 1.5$ ,  $\beta = 1.0$ ,  $E_c = 150 \text{ TeV}$ , and an energy conversion efficiency from the pulsar spin-down energy to the accelerated  $e^\pm$  energy of  $\eta \equiv W_{e^\pm}/W_{\text{sd}} = 40\% \cdot (d/1.6 \text{ kpc})^2$ . Note that the energy budget may also give an independent support of the slow diffusion scenario of the  $e^\pm$ . The one-dimensional spatial distribution of the model prediction is almost identical with the solid line in Fig. 2. The one-zone slow-diffusion model is found to give too high fluxes in GeV bands and a very hard spectrum of injected  $e^\pm$  is required, which seems to be less favored.

Note that the model flux is slightly higher than the flux measured by HAWC of 3HWC J0621+382 at median energy of  $\sim 7 \text{ TeV}$  [23]. The HAWC flux was derived assuming a disk extension of  $0^\circ.5$ , which is smaller than the extension measured by LHAASO ( $0^\circ.70$ ; see Table I). We expect that more dedicated analysis of HAWC and LHAASO-WCDA data will be very helpful in clarifying the spectral behavior below 10 TeV energies and in better constraining the model parameters.

#### V. CONCLUSIONS

Using about ten months of data recorded with the half array of the LHAASO-KM2A, we discover an extended VHE  $\gamma$ -ray source, LHAASO J0621+3755, whose location is consistent with a middle-aged pulsar, PSR J0622+3749. The source is detected with a significance of  $8.2\sigma$  above 25 TeV, and  $3.1\sigma$  above 100 TeV. LHAASO J0621+3755 is extended with a significance of  $\sim 4.1\sigma$ . A Gaussian fit gives an extension of  $\sim 0^\circ.40 \pm 0^\circ.07$ . The power-law spectral index of LHAASO J0621+3755 is  $-2.92 \pm 0.17_{\text{stat}} \pm 0.02_{\text{sys}}$ . Together with the flux upper limits from the Fermi-LAT observations, a downward-curved  $\gamma$ -ray spectrum is expected. Multi-wavelength counterparts of the LHAASO source have been searched for, and no associated sources have been found.

The LHAASO and multi-wavelength observations tend to suggest that LHAASO J0621+3755 is a pulsar halo associated with PSR J0622+3749. If the VHE  $\gamma$ -ray emission is interpreted as the ICS emission from high-energy electrons and positrons that escaped from the pulsar, the source extension indicates a diffusion coefficient of  $D(160 \text{ TeV}) \sim 8.9^{+4.5}_{-3.9} \times 10^{27} (d/1.6 \text{ kpc})^2 \text{ cm}^2 \text{ s}^{-1}$ . This is consistent with the slow diffusion scenario of particles in the turbulent medium around pulsars as inferred from the HAWC observations of Geminga and Monogem [4]. The required energy to power the VHE  $\gamma$ -ray emission is estimated to be  $\sim 20\% - 40\%$  of the pulsar spin-down energy, assuming a distance of 1.6 kpc. LHAASO J0621+3755 is thus possibly another pulsar halo besides Geminga and Monogem with extensive VHE and multi-wavelength studies and the first one with detected  $\gamma$ -ray emission up to 100 TeV energies. The discovery and measured properties of LHAASO J0621+3755 may help to establish that the diffusion of CRs in the Milky Way is inhomogeneous.

## VI. ACKNOWLEDGEMENTS

This work is supported in China by the National Key R&D program of China under the grants 2018YFA0404202, 2018YFA0404201, 2018YFA0404203, 2018YFA0404204, by the National Natural Science Foundation of China under the grants 11722328, 11851305, 11635011, 11761141001, 11765019, 11775233, U1738205, U1931111, U1931201, by Chinese Academy of Sciences, and the Program for Innova-

tive Talents and Entrepreneur in Jiangsu, and in Thailand by RTA6280002 from Thailand Science Research and Innovation. The authors would like to thank all staff members who work at the LHAASO site which is 4400 meters above sea level year-around to maintain the detector and keep the electricity power supply and other components of the experiment operating smoothly. We are grateful to Chengdu Management Committee of Tianfu New Area for the constant financial supports to research with LHAASO data.

- 
- [1] R. Trotta, G. Jóhannesson, I. V. Moskalenko, T. A. Porter, R. Ruiz de Austri, and A. W. Strong, *Astrophys. J.* **729**, 106 (2011), 1011.0037.
- [2] Q. Yuan, S.-J. Lin, K. Fang, and X.-J. Bi, *Phys. Rev. D* **95**, 083007 (2017), 1701.06149.
- [3] A. W. Strong, I. V. Moskalenko, and V. S. Ptuskin, *Annu. Rev. Nucl. Part. Sci.* **57**, 285 (2007), astro-ph/0701517.
- [4] A. U. Abeysekara, A. Albert, R. Alfaro, C. Alvarez, J. D. Álvarez, R. Arceo, J. C. Arteaga-Velázquez, D. Avila Rojas, H. A. Ayala Solares, A. S. Barber, et al., *Science* **358**, 911 (2017), 1711.06223.
- [5] M. Aguilar, D. Aisa, A. Alvino, G. Ambrosi, K. Andeen, L. Aruda, N. Attig, P. Azzarello, A. Bachlechner, F. Barao, et al., *Phys. Rev. Lett.* **117**, 231102 (2016).
- [6] K. Fang, X.-J. Bi, P.-F. Yin, and Q. Yuan, *Astrophys. J.* **863**, 30 (2018), 1803.02640.
- [7] S. Profumo, J. Reynoso-Cordova, N. Kaaz, and M. Silverman, *Phys. Rev. D* **97**, 123008 (2018), 1803.09731.
- [8] D. Hooper and T. Linden, *Phys. Rev. D* **98**, 083009 (2018), 1711.07482.
- [9] X. Tang and T. Piran, *Mon. Not. Roy. Astron. Soc.* **484**, 3491 (2019), 1808.02445.
- [10] T. Sudoh, T. Linden, and J. F. Beacom, *Phys. Rev. D* **100**, 043016 (2019), 1902.08203.
- [11] G. Giacinti, A. M. W. Mitchell, R. López-Coto, V. Joshi, R. D. Parsons, and J. A. Hinton, *Astron. Astrophys.* **636**, A113 (2020), 1907.12121.
- [12] Y. Bao, S. Liu, and Y. Chen, *Astrophys. J.* **877**, 54 (2019), 1907.02037.
- [13] Y. Bao and Y. Chen, *Astrophys. J.* **881**, 148 (2019), 1907.02038.
- [14] T. Linden, K. Auchettl, J. Bramante, I. Cholis, K. Fang, D. Hooper, T. Karwal, and S. W. Li, *Phys. Rev. D* **96**, 103016 (2017), 1703.09704.
- [15] M. Di Mauro, S. Manconi, and F. Donato, *Phys. Rev. D* **101**, 103035 (2020), 1908.03216.
- [16] M. Di Mauro, S. Manconi, M. Negro, and F. Donato, *arXiv e-prints arXiv:2012.05932* (2020), 2012.05932.
- [17] F. A. Aharonian, *Very high energy cosmic gamma radiation : a crucial window on the extreme Universe* (World Scientific Publishing, 2004).
- [18] F. A. Aharonian and A. M. Atoyan, *Astron. Astrophys.* **362**, 937 (2000), astro-ph/0009009.
- [19] T. Linden and B. J. Buckman, *Phys. Rev. Lett.* **120**, 121101 (2018), 1707.01905.
- [20] R. López-Coto and G. Giacinti, *Mon. Not. Roy. Astron. Soc.* **479**, 4526 (2018), 1712.04373.
- [21] R.-Y. Liu, H. Yan, and H. Zhang, *Phys. Rev. Lett.* **123**, 221103 (2019), 1904.11536.
- [22] K. Fang, X.-J. Bi, and P.-F. Yin, *Mon. Not. Roy. Astron. Soc.* **488**, 4074 (2019), 1903.06421.
- [23] A. Albert, R. Alfaro, C. Alvarez, J. R. A. Camacho, J. C. Arteaga-Velázquez, K. P. Arunbabu, D. Avila Rojas, H. A. Ayala Solares, V. Baghmany, E. Belmont-Moreno, et al., *arXiv e-prints arXiv:2007.08582* (2020), 2007.08582.
- [24] A. U. Abeysekara, A. Albert, R. Alfaro, C. Alvarez, J. D. Álvarez, R. Arceo, J. C. Arteaga-Velázquez, H. A. Ayala Solares, A. S. Barber, B. Baughman, et al., *Astrophys. J.* **843**, 40 (2017), 1702.02992.
- [25] H. J. Pletsch, L. Guillemot, B. Allen, M. Kramer, C. Aulbert, H. Fehrmann, P. S. Ray, E. D. Barr, A. Belfiore, F. Camilo, et al., *Astrophys. J.* **744**, 105 (2012), 1111.0523.
- [26] P. M. Saz Parkinson, M. Dormody, M. Ziegler, P. S. Ray, A. A. Abdo, J. Ballet, M. G. Baring, A. Belfiore, T. H. Burnett, G. A. Caliendo, et al., *Astrophys. J.* **725**, 571 (2010), 1006.2134.
- [27] See Supplemental Material at <https://journals.aps.org/prl/XXX> for supporting figures and tables, which includes Refs. [28–38].
- [28] X. Bai, B. Y. Bi, X. J. Bi, Z. Cao, S. Z. Chen, Y. Chen, A. Chivavassa, X. H. Cui, Z. G. Dai, D. della Volpe, et al., *arXiv e-prints arXiv:1905.02773* (2019), 1905.02773.
- [29] D. Heck, J. Knapp, J. N. Capdevielle, G. Schatz, and T. Thouw, *CORSIKA: a Monte Carlo code to simulate extensive air showers*. (TIB Hannover, 1998).
- [30] S. Chen, in *36th International Cosmic Ray Conference (ICRC2019)* (2019), vol. 36 of *International Cosmic Ray Conference*, p. 219.
- [31] S. Agostinelli, J. Allison, K. Amako, J. Apostolakis, H. Araujo, P. Arce, M. Asai, D. Axen, S. Banerjee, G. Barend, et al., *Nuclear Instruments and Methods in Physics Research A* **506**, 250 (2003).
- [32] H. T. Intema, P. Jagannathan, K. P. Mooley, and D. A. Frail, *Astron. Astrophys.* **598**, A78 (2017), 1603.04368.
- [33] E. L. Wright, P. R. M. Eisenhardt, A. K. Mainzer, M. E. Ressler, R. M. Cutri, T. Jarrett, J. D. Kirkpatrick, D. Padgett, R. S. McMillan, M. Skrutskie, et al., *Astron. J.* **140**, 1868 (2010), 1008.0031.
- [34] B. M. Lasker, C. R. Sturch, B. J. McLean, J. L. Russell, H. Jenkner, and M. M. Shara, *Astron. J.* **99**, 2019 (1990).
- [35] R. D’Abrusco, F. Massaro, A. Paggi, H. A. Smith, N. Masetti, M. Landoni, and G. Tosti, *Astrophys. J. Supp.* **215**, 14 (2014), 1410.0029.
- [36] F. Massaro, M. Giroletti, R. D’Abrusco, N. Masetti, A. Paggi, P. S. Cowperthwaite, G. Tosti, and S. Funk, *Astrophys. J. Supp.* **213**, 3 (2014), 1503.03483.
- [37] M. Ackermann, M. Ajello, A. Albert, W. B. Atwood, L. Baldini, J. Ballet, G. Barbiellini, D. Bastieri, K. Bechtol, R. Bellazzini, et al., *Astrophys. J.* **799**, 86 (2015), 1410.3696.

- [38] A. M. Atoyan, F. A. Aharonian, and H. J. Völk, *Phys. Rev. D* **52**, 3265 (1995).
- [39] F. Aharonian, Q. An, Axikegu, L. X. Bai, Y. X. Bai, Y. W. Bao, D. Bastieri, X. J. Bi, Y. J. Bi, H. Cai, et al., arXiv e-prints arXiv:2010.06205 (2020), 2010.06205.
- [40] K. Greisen, *Annual Review of Nuclear Science* **10**, 63 (1960).
- [41] K. Kawata, T. K. Sako, M. Ohnishi, M. Takita, Y. Nakamura, and K. Munakata, *Experimental Astronomy* **44**, 1 (2017).
- [42] A. U. Abeysekara, A. Albert, R. Alfaro, C. Alvarez, J. D. Álvarez, J. R. A. Camacho, R. Arceo, J. C. Arteaga-Velázquez, K. P. Arunbabu, D. Avila Rojas, et al., *Astrophys. J.* **881**, 134 (2019), 1905.12518.
- [43] M. Amenomori, S. Ayabe, D. Chen, S. W. Cui, Danzengluobu, L. K. Ding, X. H. Ding, C. F. Feng, Z. Y. Feng, X. Y. Gao, et al., *Astrophys. J.* **633**, 1005 (2005).
- [44] M. Amenomori, S. Ayabe, X. J. Bi, D. Chen, S. W. Cui, Danzengluobu, L. K. Ding, X. H. Ding, C. F. Feng, Z. Feng, et al., *Science* **314**, 439 (2006), astro-ph/0610671.
- [45] S. S. Wilks, *Annals of Mathematical Statistics* **9**, 60 (1938).
- [46] Y. Zhang, R.-Y. Liu, S. Z. Chen, and X.-Y. Wang, arXiv e-prints arXiv:2010.15731 (2020), 2010.15731.
- [47] P. L. Nolan, A. A. Abdo, M. Ackermann, M. Ajello, A. Allafort, E. Antolini, W. B. Atwood, M. Axelsson, L. Baldini, J. Ballet, et al., *Astrophys. J. Supp.* **199**, 31 (2012), 1108.1435.
- [48] M. Di Mauro, S. Manconi, and F. Donato, *Phys. Rev. D* **100**, 123015 (2019), 1903.05647.
- [49] S. P. Wakely and D. Horan, *International Cosmic Ray Conference* **3**, 1341 (2008).
- [50] S. Abdollahi, F. Acero, M. Ackermann, M. Ajello, W. B. Atwood, M. Axelsson, L. Baldini, J. Ballet, G. Barbiellini, D. Bastieri, et al., *Astrophys. J. Supp.* **247**, 33 (2020), 1902.10045.
- [51] P. C. Gregory, W. K. Scott, K. Douglas, and J. J. Condon, *Astrophys. J. Supp.* **103**, 427 (1996).
- [52] C. G. T. Haslam, C. J. Salter, H. Stoffel, and W. E. Wilson, *Astron. Astrophys. Supp.* **47**, 1 (1982).
- [53] W. Reich, *Astron. Astrophys. Supp.* **48**, 219 (1982).
- [54] E. M. Berkhuijsen, *Astron. Astrophys. Supp.* **5**, 263 (1972).
- [55] J. J. Condon, J. J. Broderick, G. A. Seielstad, K. Douglas, and P. C. Gregory, *Astron. J.* **107**, 1829 (1994).
- [56] S.-Q. Xi, R.-Y. Liu, Z.-Q. Huang, K. Fang, and X.-Y. Wang, *Astrophys. J.* **878**, 104 (2019), 1810.10928.
- [57] H.-M. Zhang, S.-Q. Xi, R.-Y. Liu, Y.-L. Xin, S. Liu, and X.-Y. Wang, *Astrophys. J.* **889**, 12 (2020), 1909.13185.
- [58] R. N. Manchester, G. B. Hobbs, A. Teoh, and M. Hobbs, *Astron. J.* **129**, 1993 (2005), astro-ph/0412641.
- [59] G. G. Pavlov, D. Sanwal, and V. E. Zavlin, *Astrophys. J.* **643**, 1146 (2006), astro-ph/0511364.
- [60] L. Bîrzan, G. G. Pavlov, and O. Kargaltsev, *Astrophys. J.* **817**, 129 (2016), 1511.03846.